First limit on WIMP cross section with low background CsI(Tℓ) crystal detector

KIMS Collaboration

H.S. Lee [a,*], H. Bhang [a], J.H. Choi [a], I.S. Hahn [d], D. He [f], M.J. Hwang [c], H.J. Kim [e], S.C. Kim [a], S.K. Kim [a], S.Y. Kim [a], T.Y. Kim [a], Y.D. Kim [b], J.W. Kwak [a], Y.J. Kwon [c], J. Lee [a], J.H. Lee [a], J.I. Lee [b], M.J. Lee [a], J. Li [f,g], S.S. Myung [a], H. Park [a,1], H.Y. Yang [a], J.J. Zhu [f]

[a] *DMRC and School of Physics, Seoul National University, Seoul 151-742, South Korea*
[b] *Department of Physics, Sejong University, Seoul 143-747, South Korea*
[c] *Physics Department, Yonsei University, Seoul 120-749, South Korea*
[d] *Department of Science Education, Ewha Womans University, Seoul 120-750, South Korea*
[e] *Physics Department, Kyungpook National University, Daegu 702-701, South Korea*
[f] *Department of Engineering Physics, Tsinghua University, Beijing 100084, China*
[g] *Institute of High Energy Physics, Chinese Academy of Sciences, Beijing 100039, China*

Abstract

The Korea Invisible Mass Search (KIMS) Collaboration has been carrying out WIMP search experiment with CsI(Tℓ) crystal detectors at the YangYang Underground Laboratory. A successful reduction of the internal background of the crystal was done and a good pulse shape discrimination was achieved. We report the first result on WIMP search obtained with 237 kg days data using one full-size CsI(Tℓ) crystal of 6.6 kg mass.

© 2005 Elsevier B.V. Open access under CC BY license.

PACS: 29.40.Mc; 14.80.Ly; 95.35.+d

Keywords: WIMP; Dark matter; CsI(Tℓ) crystal; Pulse shape discrimination; KIMS

1. Introduction

Although the existence of dark matter as a major portion of the matter in the universe has been well supported by various astronomical observations, its identity is unknown yet. Weakly interacting massive particle (WIMP) is regarded as one of the strongest candidates for cold dark matter particle [1] and many experimental searches for WIMPs have been performed. An indication of an annual modulation of the signal reported by DAMA using NaI(Tℓ) crystal detectors may be a possible evidence of WIMP signal [2]. However, stringent limits set by cryogenic detectors, CDMS [3] and EDELWEISS [4] seem to rule out the DAMA signal region. Still, ways of interpreting both results without conflict are not completely excluded because of the difference in experimental techniques and target nuclei [5–7].

The Korea Invisible Mass Search (KIMS) Collaboration has been carrying out the WIMP search with CsI(Tℓ) crystals. Low threshold suitability for WIMP search and pulse shape discrimination (PSD) superiority to NaI(Tℓ) has been demonstrated [8–11]. Even if the CsI(Tℓ) crystal has the advantage of a good

---

* Corresponding author.
 E-mail addresses: tgsh@hep1.snu.ac.kr (H.S. Lee), skkim@hep1.snu.ac.kr (S.K. Kim).
 [1] Present address: Division of Chemical Metrology and Materials Evaluation, Korea Research Institute of Standards and Science, Yuseong, Daejeon 305-600, Republic of Korea.

PSD and the ease of getting a large detector mass, the internal background including ^{137}Cs, ^{134}Cs and ^{87}Rb has been a major hurdle to apply the crystal to WIMP search [11,12]. We have successfully purified CsI(Tℓ) crystals after extensive studies on the contamination mechanism. A pilot experiment with a low background CsI(Tℓ) crystal of 6.6 kg mass has been carried out at the YangYang Underground Laboratory (Y2L) in Korea. We report the first result obtained with 237 kg days of data taken with one crystal of $8 \times 8 \times 23$ cm^3.

2. YangYang underground laboratory

We have established an underground laboratory at YangYang utilizing the space provided by the YangYang Pumped Storage Power Plant currently under construction by Korea Midland Power Co. The underground laboratory is located in a tunnel where the vertical earth overburden is approximately 700 m. The muon flux measured with the muon detector is 2.7×10^{-7}/cm^2/s, which is consistent with the water equivalent depth of 2000 m [13]. The laboratory is equipped with a clean room with an air conditioning system for a constant temperature and low humidity. An environment monitoring system is installed for continuous monitoring of temperature and humidity. The temperature inside the CsI(Tℓ) detector container is stable within ± 0.2 °C. The rock composition surrounding the laboratory was analyzed with the ICP-MASS method and the contamination of ^{238}U and ^{232}Th is reported to be at a level of < 0.5 ppm and 5.6 ± 2.6 ppm, respectively. The relatively low contamination of ^{238}U in the rocks of the tunnel results in a low level of radon contamination in the air of the tunnel. A radon detector [14] was constructed to monitor the level of radon in the experimental hall. The contamination level of ^{222}Rn in the tunnel air was 1–2 pCi/ℓ which is slightly lower than other underground laboratories such as Gran Sasso [15] and Kamiokande [16]. The neutron flux in the experimental hall is continuously measured with two one-liter BC501A liquid scintillation detectors inside and outside of the main shield. The estimated neutron flux in the experimental hall is 8×10^{-7}/cm^2/s for 1.5 MeV $< E_{neutron} < 6.0$ MeV which is much lower than that in the Cheongpyung Underground Laboratory [17].

3. Reduction of the internal background in CsI(Tℓ) crystal

The major radioisotopes in the CsI(Tℓ) crystal contributing to the internal background are ^{137}Cs, ^{134}Cs and ^{87}Rb [12, 18]. ^{134}Cs has a half-life of 2 years and has a cosmogenic origin-neutron capture by ^{133}Cs. Therefore, ^{134}Cs is unavoidable unless the crystals are stored underground for many years. However the signal from its decay can be easily removed by the γ-ray that follows immediately after the β decay. The signal is large and beyond the energy range of our interest for WIMP search. Additional reduction can be made by using coincidence signals from neighboring crystals. The average contamination level of ^{134}Cs is measured to be 20 mBq/kg, while 1 mBq/kg can contribute only less than 0.07 counts/(keV kg day) (CPD)

at 10 keV. Therefore the ^{134}Cs contamination is not a major problem.

^{137}Cs, the half-life of which is 30 years, comes from a man-made origin, mainly due to nuclear bombs and nuclear reactors. It decays to an excited state of ^{137}Ba by emitting an electron with a Q value of 514 keV, followed by γ-ray emission to the ground state ^{137}Ba with a half-life of 2.55 minutes. Therefore the Compton scattering of this γ-ray as well as the β-ray can cause background in the low energy range where WIMP signals are expected. Simulation studies show that 1 mBq/kg can contribute 0.35 CPD background in the 10 keV region. We investigated the contamination process and the reduction method of ^{137}Cs. Most of the suspected intermediate products from pollucite, an ore of Cs, to CsI powder has been measured with a low background HPGe detector installed at the Y2L. We also investigated the processing water and conclude that the main source of ^{137}Cs is the processing water used for the powder production, in which the contamination level of ^{137}Cs was found to be 0.1 mBq/ℓ. By using purified water, we succeeded in reducing the ^{137}Cs in the final powder and the crystal [18].

Rb, which includes 27.8% of ^{87}Rb, exists in the pollucite at a 0.7% level and can contaminate easily because it is chemically similar to Cs. The ^{87}Rb undergoes β decay to the ground state of its daughter nucleus, ^{87}Sr, with emission of an electron whose end point energy is 282 keV. This can be a very serious background, and 1 ppb contamination can contribute 1.07 CPD at 10 keV. Contamination of many CsI powders in the market has been measured with the ICP-MASS method and we found that it varies from 1 to 1000 ppb. The reduction technique of Rb, a repeated recrystallization process, has been widely known. We performed the recrystallization to the powder that we obtained with pure water and reduced the Rb contamination below 1 ppb. The reduction of the internal background is discussed in detail elsewhere [19].

4. Experimental setup

We have installed a shielding structure in the experimental hall to stop the external background originating mainly from the surrounding rocks. The shield consists of 10 cm thick oxygen free high conductivity (OFHC) copper, 5 cm thick polyethylene (PE), 15 cm thick boliden lead and 30 cm mineral oil (liquid parafin) from inside out. The mineral oil is mixed with 5% of a pseudocumene-based liquid scintillator and mounted with PMTs so that it can perform as a muon detector [13]. Inside the copper chamber, N$_2$ gas is flown at a rate of 4 ℓ/min to reduce the radon contamination as well as to keep the humidity low.

The CsI(Tℓ) crystal (full-size crystal) used for the experiment has a dimension of $8 \times 8 \times 23$ cm^3 and a mass of 6.6 kg. The crystal is attached with two low background quartz window PMTs with RbCs photocathode. RbCs photocathode enhances quantum efficiency in the green wavelength region and gives 50% more photo-electron yield for CsI(Tℓ) crystal than a normal bialkali PMT does. As a result, the number of photo-electrons is about 5.5/keV for the full-size crystal.

The signal from the PMT is amplified with a preamplifier mounted outside the main shield and brought to the FADC mod-
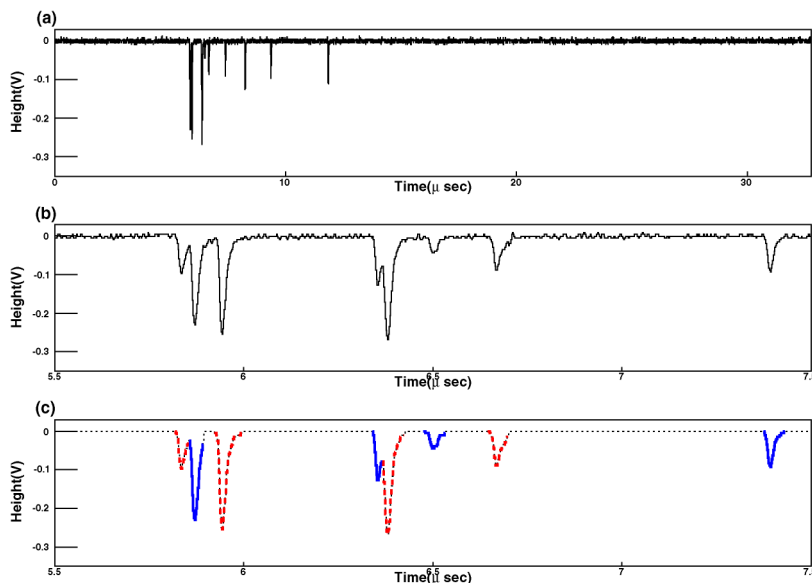
Fig. 1. (a) shows typical low energy γ signal from CsI(Tℓ) crystal for one PMT obtained by Compton events from ^{137}Cs source. Zoomed pulse shape of this event from 5.5 to 7.5 µs is shown at (b). The same pulse spectrum with clustering is shown in (c). The neighboring cluster is separated by a different style (solid line and dashed line).

ule through a 20 m-long coaxial cable. The homemade FADC module is designed to sample the pulse every 2 ns for a duration up to 32 µs so that one can fully reconstruct each photo-electron pulse as shown in Fig. 1. The trigger is formed in the FPGA chip on the FADC board. For low energy events, it is required to have more than five photoelectrons in two µs for the event trigger. An additional trigger is generated if the width of the pulse is longer than 200 ns for high energy events where many single photon signals are merged into a big pulse. The FADC located in a VME crate is read out by a Linux-operating PC through the VME-USB2 interface with a maximum data transfer rate of 10 Mbytes/s. The DAQ system is based on the ROOT [20] package.

During the two-month period starting from July 2004, we have taken data for WIMP search using one crystal with a background level of approximately 7 CPD at 10 keV. The amount of data was 237 kg days.

5. Calibration data

The different timing characteristics between nuclear recoil and electron recoil in CsI(Tℓ) crystal make it possible to statistically separate the nuclear recoil events from the γ background using the mean time distribution [9–11]. In order to have a good reference distribution of the mean time for them, we took calibration data of electron recoil from the γ source and nuclear recoil from the neutron source.

The γ calibration data was obtained with a full-size crystal by a ^{137}Cs source in the copper chamber of Y2L. Identical setup and conditions as for the WIMP search data were used. For one week irradiation, we took low energy γ-ray events equivalent to approximately 3000 kg days WIMP search data.

Neutron calibration data were obtained by exposing a small-size test crystal ($3 \times 3 \times 3$ cm^3) to neutrons from 300 mCi

Am–Be source, prepared at Seoul National University [21]. In order to identify neutrons scattered from CsI, we used neutron detectors, made of BC501A contained in a cylindrical stainless steel vessel. Each neutron detector is shielded by 5 cm lead and 10 cm paraffin, and set up at various angles with respect to the incident neutron direction. The Am–Be source is surrounded by liquid scintillator (LSC) composed of 95% mineral oil and 5% of pseudocumene with a collimation hole to the direction of the CsI(Tℓ) crystal. The LSC acts as a tagging detector of 4.4 MeV γ's which are simultaneously generated with neutrons from the Am–Be source as well as a neutron shield for the low surface neutron flux outside of the source.

In order to identify neutron-induced events, we required a coincidence between any one of the neutron detectors and the CsI(Tℓ) crystal. With a good neutron separation capability, we took neutron data, whose amount depended on energy, equivalent to approximately 1200 kg days WIMP search data at 3–11 keV.

We also took electron recoil data using a ^{137}Cs source for the test crystal used for the neutron calibration. This data is compared with the electron recoil calibration data obtained for the full-size crystal to confirm that neutron calibration data can be used for the full-size crystal.

6. Data analysis

Single photo-electrons (SPEs) in an event is identified by applying a clustering algorithm to the FADC data. The energy deposition is evaluated from the sum of charges of all SPEs in the event. Also, using the time information of SPEs we calculate mean time (MT). The MT distribution of events above 3 keV and up to 11 keV is used to extract the fraction of nuclear recoil events for WIMP search.
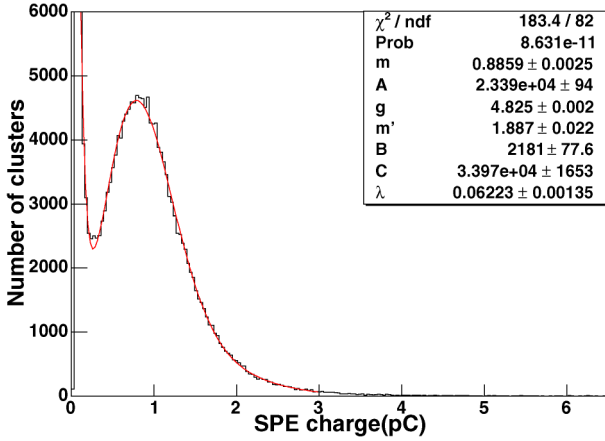
Fig. 2. Single cluster charge spectrum. The distribution is fitted with two Poisson functions.

As one can see in Fig. 1(b), the single clusters of low energy events are well reconstructed in our DAQ system. A clustering algorithm to identify each SPE signal is applied for the data analysis. The clustering algorithm includes the identification of local maximum to form isolated cluster using the FADC bins above the pedestal and the separation of neighboring cluster in the case two local maximum is found in a cluster. A threshold is applied to the pulse height to select SPE candidate. Additionally the SPE candidate with an unusually narrow pulse width out of 3σ is rejected. Fig. 1(c) shows result of clustering of (b). The sum of the single cluster charges for whole window (32 μs) are used to calculate the deposited energy. Low energy calibration is done using a 59.5 keV γ peak from ^{241}Am.

Fig. 2 shows the charge distribution of single cluster after clustering of 5.9 keV peak from a ^{55}Fe source without height threshold. The distribution is fitted by two superimposed Poisson functions (one for the SPE and the other for the SPE-overlapped signal) with exponential noise component:

$$f = A \frac{\mu^r e^{-\mu}}{\Gamma(r+1)} + B \frac{\mu'^r e^{-\mu'}}{\Gamma(r+1)} + C e^{-x/\lambda},$$
$$r = xg, \qquad \mu = mg, \qquad \mu' = m'g$$

where $m (m')$ is the mean of the Poisson distribution, and g is the gain factor of the PMT. The fitting function is overlaid in the figure as a solid line. The ratio of the contribution of the two Poisson distributions is 9.3%. Therefore, we conclude that $\sim 90\%$ of SPEs make single clusters and $\sim 10\%$ makes overlapped clusters. The ratio of the mean values of the two Poisson distributions, m'/m, is 2.11 ± 0.03 which is consisted with a expectation considering overlap of up to 3-SPEs. In this fit, the most probable value (MPV) of the SPE is obtained as 0.86 pC. From the total charge of 59.5 keV from a ^{241}Am source, the photo-electron yield of this crystal is obtained as 5.5/keV.

The photo-electron yield is calibrated at the beginning and at the end of a run. The results show stability of the light output within 1% for the whole period. The time-dependent gain variation is corrected by the MPV which is obtained from the SPE charge spectrum of low energy (4–8 keV) WIMP search data and its Poisson fit. Every one week's WIMP search data are accumulated to the fit. The result shows that the gain is stable within 5% for each PMT in the whole period.

The PMT noise, which was also detected without the crystal, is seen by both PMTs which have very fast timing characteristics. A similar noise was reported by another group [22].
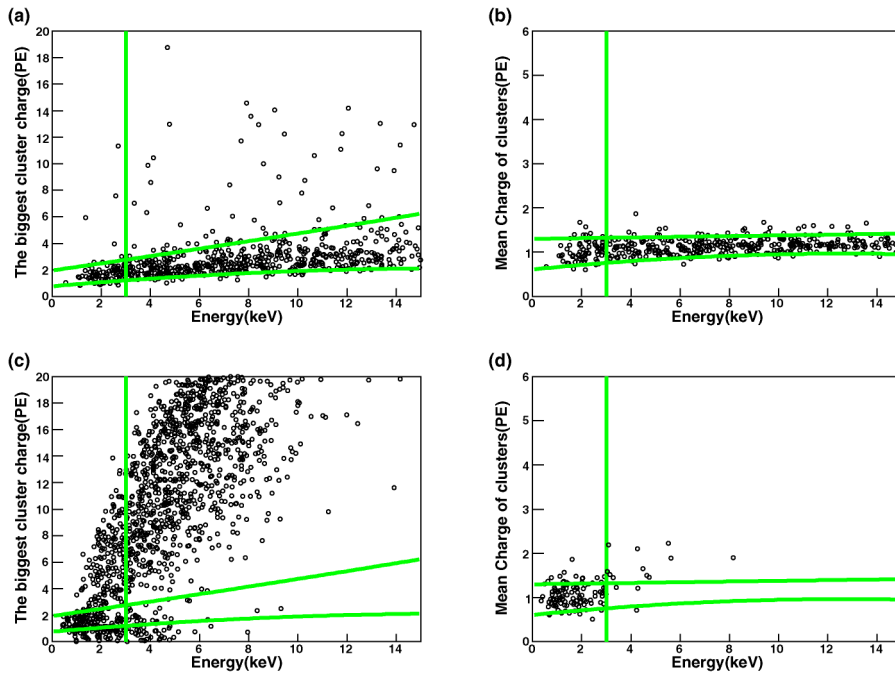

Fig. 3. (a) shows the charge of the biggest cluster normalized by the MPV of the SPE charge obtained from Fig. 2 fit, versus the measured energy for the calibration data with a ^{137}Cs γ source. Two solid lines indicate -1.65σ (lower solid line) and 1.28σ band (upper solid line). The vertical line is the 3 keV analysis threshold. (b) is a similar spectrum for the mean charge of clusters for the events within the signal band of the biggest cluster cut. (c) and (d) are the corresponding plots for PMT noise events.

It seems to be originated from a spark in the dynode structure [23]. The PMT noise usually induces an abnormally big cluster. Therefore, the charge of the biggest cluster and the mean charge of clusters for each event can be used to reject these events. We construct a good event-band using the Compton scattering events from ^{137}Cs, and they are compared with PMT noise events in Fig. 3. PMT noise events were taken from the same system without the CsI(Tℓ) crystal in the copper chamber. The distance between the two PMTs is maintained equal to that for the crystal-attached set-up. In the 25.4 days data, equivalent to 167 kg days WIMP search data, only two events passed all the cuts with the 3 keV energy threshold. We conclude that the PMT background after the cuts is negligible. The same cut is applied to the Compton scattering data and the efficiency was found to be approximately 60% independent of energy as shown in Fig. 4.

We applied the same cuts to the calibration data taken with the test crystal. The efficiency of ^{137}Cs and the neutron calibration data for the test crystal are compared with ^{137}Cs data for the full-size crystal in Fig. 4. About a 10% difference between the full-size and test crystals is observed. This is mainly due to the different PMTs used. We assign a systematic uncertainty in efficiency to account for this difference. With a similarity of efficiency for neutron and the γ calibration data in test crystal, we can conclude that we can use γ calibration data for efficiency calculations of WIMP search data. A slight difference in efficiency between γ and neutron data is also included as a systematic uncertainty. The systematic error for the efficiency calculation is summed as

$$\sigma_{sys}^2 = \sigma_{crystal\ diff}^2 + \sigma_{recoil\ diff}^2$$

where $\sigma_{crystal\ diff}$ is efficiency difference between the full-size crystal and the test crystal, $\sigma_{recoil\ diff}$ is the efficiency difference between the nuclear recoil and the γ recoil events. Efficiency corrected energy spectrum of events before and after the cuts are shown in Fig. 5. Events below 11 keV are used for the WIMP search.

To estimate the WIMP signal fraction in the WIMP search data, we introduce a mean time (MT) value which is defined as

$$\langle t \rangle = \frac{\sum A_i t_i}{\sum A_i} - t_0$$

where A_i and t_i are the charge and the time of the ith cluster respectively, and t_0 is the time of the first cluster (assumed as time zero).

Because we use different crystals for the neutron calibration, we need to confirm whether the two different crystals show the same MT characteristics. The ^{137}Cs calibration data of the test crystal is compared with that of the full-size crystal. As one can see in Fig. 6, the MT distribution of Compton electrons in the test crystal is well matched with that of the full-size crystal. The mean value of the log(MT) distribution as a function of energy is shown in Fig. 7. An excellent agreement between the test crystal and the full-size crystal for the Compton electron allows us to use the neutron signal from the test crystal as a reference for nuclear recoil signal for the full-size crystal. A slight MT difference is adjusted by the assumption of a constant $R_\tau =$
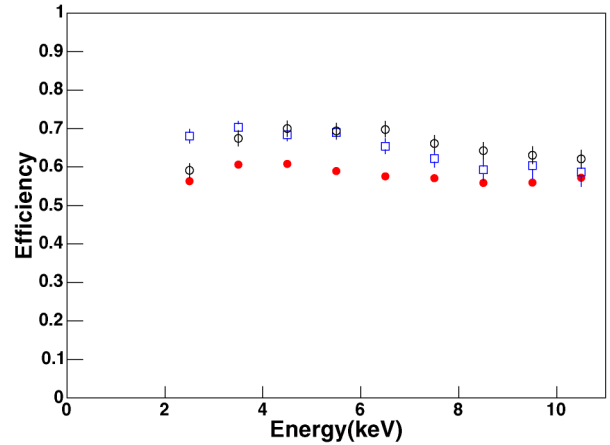

Fig. 4. Efficiency calculated with γ calibration data for full-size crystal (filled circles), test crystal (open circles), and neutron calibration data for test crystal (open square) where only statistical errors are included.
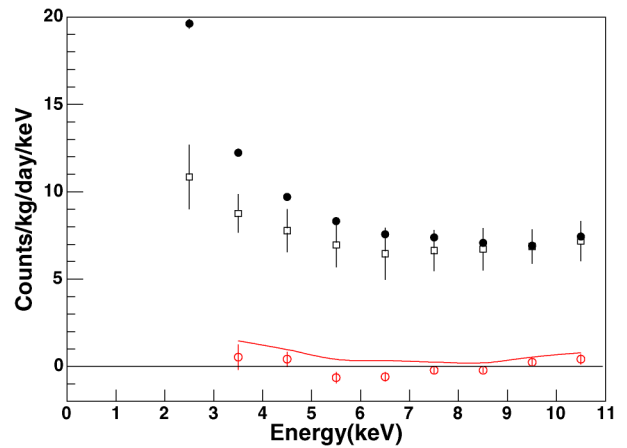

Fig. 5. Energy spectrum in WIMP signal region before applying cuts (filled circles), the big cluster events rejection with efficiency correction (open squares), and fitted nuclear recoil rate (open circles) where the errors include systematic uncertainty of efficiency for the latter two cases. A 90% upper limit on the nuclear recoil rate is shown with a solid line.
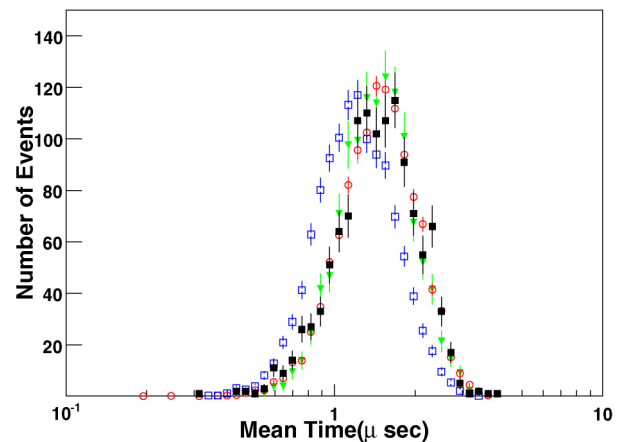

Fig. 6. Mean time distributions of Compton electrons for the test crystal (filled triangles) and full-size crystal (open circles) in the 4–5 keV energy range are compared. Also, we include nuclear recoil (open squares), and the WIMP search data (filled squares) for comparison.
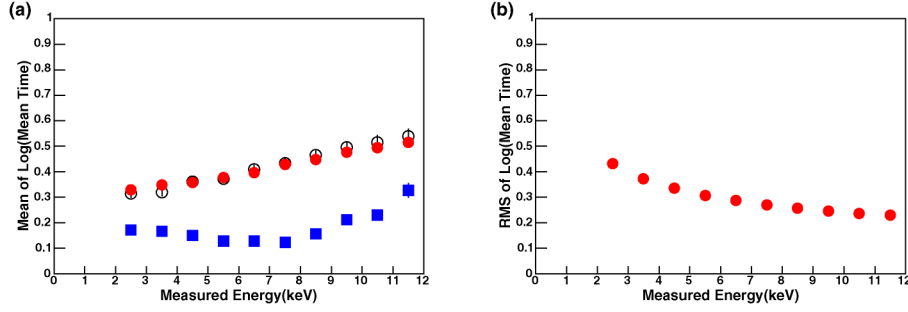
Fig. 7. (a) The mean value of log(MT) as a function of measured energy for Compton electrons with the test crystal (open circles), with the full-size crystal (filled circles), and for the nuclear recoil with the test crystal (filled squares). (b) Root mean square (RMS) of log(MT) as a function of measured energy for Compton electrons with the full-size crystal.

τ_n/τ_e [22]. Where τ_n is the MT of the nuclear recoil and τ_e is the MT of the electron recoil.

Since the MT distribution depends significantly on the measured energy in the low energy region, the log(MT) distribution in each keV energy bin is fitted to the reference distribution for the same energy bin. The fitted nuclear recoil event rate after the efficiency correction is given in Fig. 5. The fitted nuclear recoil event rates are consistent with zero within one standard deviation error for all energy bins. A 90% confidence level (CL) upper limit on nuclear recoil event rates are shown with a solid line. Since below 3 keV the PMT background contributes significantly and the pulse shape discrimination power is less effective, we do not use events below 3 keV. In order to evaluate nuclear recoil energy one needs to know the quenching factor (QF) defined by the γ equivalent measured energy divided by the nuclear recoil energy. We used the QF measured in our previous beam test [9]. Our threshold of 3 keV corresponds to 20 keV nuclear recoil energy.

7. Result and discussion

Assuming a Maxwellian dark matter velocity distribution with a spherical halo model discussed in Ref. [24], the total WIMP rate is obtained as

$$R(E_0, E_\infty)$$
$$= \frac{k_0}{k_1} \int_0^\infty dE_R \left\{ c_1 \frac{R_0}{E_0 r} e^{-c_2 E_R/E_0 r} - \frac{R_0}{E_0 r} e^{-v_{esc}^2/v_0^2} \right\},$$

$$R_0 = 5.47 \left(\frac{\text{GeV}/c^2}{m_\chi} \right) \left(\frac{\text{GeV}/c^2}{m_t} \right) \left(\frac{\sigma_0}{\text{pb}} \right)$$
$$\times \left(\frac{\rho_\chi}{\text{GeV}/c^2/\text{cm}^3} \right) \left(\frac{v_0}{\text{km/s}} \right)$$

$$E_0 = \frac{1}{2} m_\chi v_0^2, \qquad r = \frac{4 m_\chi m_t}{(m_\chi + m_t)^2} \tag{1}$$

where R_0 is the event rate per kg day for $v_E = 0$ and $v_{esc} = \infty$, $v_{esc} = 650$ km/s is the local Galactic escape velocity of WIMP, m_t is the mass of a target nucleus, $\rho_\chi = 0.3$ GeV/cm^3 is local dark matter density, $v_0 = 220$ km/s is a Maxwell velocity parameter, and c_1, c_2 are constants, as discussed in Ref. [24].

In order to estimate the expected event rates for each energy bin, we use MC simulation. The MC simulation based on

GEANT4 [25] takes into account the recoil energy spectrum, the QF, and the light transportation to the PMTs. Then the simulated events are analyzed in the same way as the data except for the applying any analysis cuts. The energy is tuned to provide good agreement with the calibration data using 59.5 keV γ-rays from a ^{241}Am source. Fig. 8(a) shows good agreement between Monte Carlo and calibration data for the energy distribution. The Monte Carlo generated electron equivalent energy distributions (E_{ee}) for several WIMP masses are shown in Fig. 8(b).

From the rate of nuclear recoil in each energy bin, we can estimate the total WIMP rate in comparison with the simulated E_{ee} distribution for each WIMP mass by the following relation.

$$R(E_0, E_\infty) = R_{E_k} N_{\text{total}}/N_{E_k} \tag{2}$$

where R_{E_k} and N_{E_k} are the measured nuclear recoil rate and the simulated WIMP events for each energy bin E_k respectively and, N_{total} is the total number of WIMP events generated by simulation. With Eqs. (1) and (2), we can convert the rate of nuclear recoil in each energy bin to the WIMP-nucleus cross section for each WIMP mass.

The limits on the cross-section for various energy bins and targets (Cs and I) have been combined following the procedure described in Ref. [24] assuming the measurements for different energy bins are statistically independent. The combined result from energy bins for a WIMP-nucleus cross section is obtained from this expression

$$\sigma_{W-A} = \frac{\sum \sigma_{W-A}(E_k)/\delta\sigma_{W-A}^2(E_k)}{\sum 1/\delta\sigma_{W-A}^2(E_k)},$$
$$\frac{1}{\delta\sigma_{W-A}^2} = \sum \frac{1}{\delta\sigma_{W-A}^2(E_k)} \tag{3}$$

where σ_{W-A} is a combined WIMP-nucleus cross section, $\sigma_{W-A}(E_k)$ is a WIMP-nucleus cross section calculated in an energy bin E_k. As one can see in Fig. 5, the rate of nuclear recoil events is consistent with zero. Therefore, we can set the 90% CL upper limit on the WIMP-nucleus cross section with Eq. (3). In this process, we assign zero as the mean value for the event rate for the bins with negative means. The WIMP-nucleon cross section can be obtained from WIMP-nucleus cross section by following equation

$$\sigma_{W-n} = \sigma_{W-A} \frac{\mu_n^2}{\mu_A^2} \frac{C_n}{C_A} \tag{4}$$
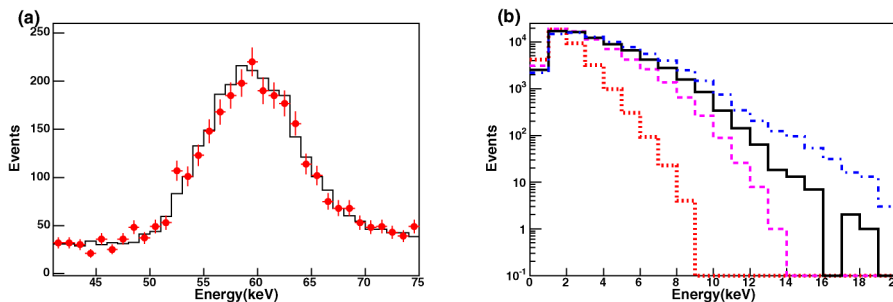
Fig. 8. (a) Distribution of E_{ee} for the MC simulation (solid line) and calibration data (filled circles) for a ^{241}Am source are compared. (b) Simulated E_{ee} spectra for several WIMP masses (20 MeV—dotted line, 50 MeV—dashed line, 100 MeV—solid line, 1000 MeV—dotted dashed line) are shown.

where $\mu_{n,A}$ are the reduced masses of WIMP-nucleon and WIMP-target nucleus of mass number A and $C_A/C_n = A^2$ for spin independent interaction. The limit on the WIMP-nucleon cross section for each nucleus can be combined by this expression

$$\frac{1}{\sigma} = \frac{1}{\sigma_{Cs}} + \frac{1}{\sigma_I}. \tag{5}$$

A 90% CL upper limit on the WIMP-nucleon cross section from CsI for spin independent interaction is shown in Fig. 9, together with the limits obtained from two NaI(Tℓ) crystal based WIMP search experiments with similar pulse shape analyses, NAIAD (UKDMC) [22] and DAMA [26]. Although the amount of data used to get our limit is 10 times less than that of NAIAD, we achieved a more stringent limit than that of NAIAD due to the better pulse shape discrimination and lower recoil energy threshold.
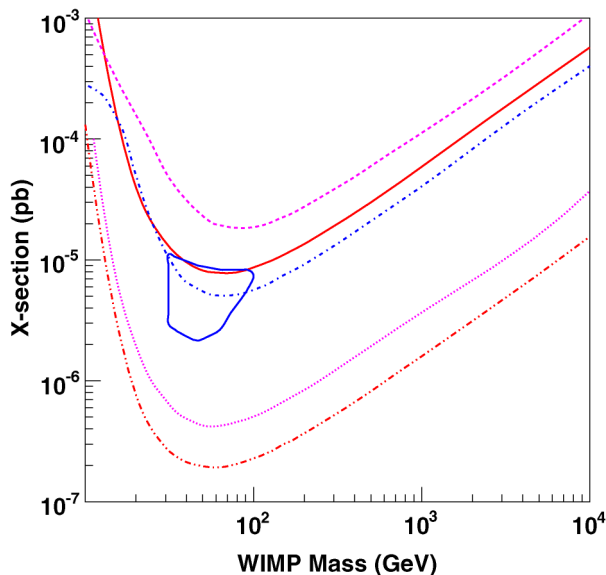

Fig. 9. The KIMS limit on a WIMP-nucleon cross section for a spin independent interaction with 237 kg days exposure (solid line), DAMA positive [2] annual modulation signal (closed curve), NAIAD limit [22] with 3879 kg days exposure (dashed line) and, DAMA limit [26] with 4123 kg days (dashed-dotted line) are presented. Also the KIMS projected limit with 250 kg year exposure of 2 CPD background level (dashed-double-dotted line) is presented. Dotted line shows current best limit by CDMS group [3].

8. Conclusion

The KIMS Collaboration has developed a low background CsI(Tℓ) crystal for the WIMP search. We set the first limit on the WIMP cross section using the 237 kg days data taken with a 6.6 kg crystal. Our limit already partially excludes the DAMA 3σ signal region. The current experimental setup is designed to accommodate about 250 kg of CsI(Tℓ) crystals without any modification. We expect that the background rate will be reduced to the level of approximately 2 CPD or less for the new powder produced with purer water. The projected limit for 1 year of data taken with 250 kg crystals of 2 CPD background is shown in Fig. 9 in comparison with the current best limit set by CDMS [3]. With the 250 kg setup, KIMS can explore the annual modulation as well.

References

[1] G. Jungman, M. Kamionkowski, K. Griest, Phys. Rep. 267 (1996) 195.
[2] R. Bernabei, et al., Phys. Lett. B 480 (2000) 23.
[3] D.S. Akerib, et al., Phys. Rev. Lett. 93 (2004) 211301.
[4] S. Marnieros, et al., Nucl. Instrum. Methods A 520 (2004) 101.
[5] R. Bernabei, et al., Int. J. Mod. Phys. D 13 (2004) 2127.
[6] R. Foot, Mod. Phys. Lett. A 19 (2004) 1841.
[7] F. Giuliani, Phys. Rev. Lett. 93 (2004) 161301;
    C. Savage, et al., Phys. Rev. D 70 (2004) 123513.
[8] H.J. Kim, et al., Nucl. Instrum. Methods A 457 (2001) 471.
[9] H. Park, et al., Nucl. Instrum. Methods A 491 (2002) 460.
[10] S. Pecourt, et al., Astropart. Phys. 11 (1999) 457.
[11] V.A. Kudryavtsev, et al., Nucl. Instrum. Methods A 456 (2001) 272.
[12] T.Y. Kim, et al., Nucl. Instrum. Methods A 500 (2003) 337.
[13] J.J. Zhu, et al., High Energy Phys. Nucl. Phys. 29 (2005) 721.
[14] M.J. Lee, et al., in preparation.
[15] A. Bassignani, et al., Radiat. Meas. 25 (1995) 557.
[16] S. Fukuda, et al., Nucl. Instrum. Methods A 501 (2003) 418.
[17] H.J. Kim, et al., Astropart. Phys. 20 (2004) 549.
[18] Y.D. Kim, et al., J. Korean Phys. Soc. 40 (2002) 520;
    Y.D. Kim, et al., Nucl. Instrum. Methods A 552 (2005) 456.

[19] H.S. Lee, et al., in: Proceedings of the 5th International Workshop on the Identification of Dark Matter, World Scientific, 2004, p. 390.

[20] R. Brunn, F. Rademakers, ROOT—an object oriented data analysis framework, in: Proceedings of AIHENP '96 Workshop, Lausanne, September 1996, Nucl. Instrum. Methods A 389 (1997) 81, see also http://root.cern.ch.

[21] J. Lee, et al., in preparation.

[22] B. Ahmed, et al., Astropart. Phys. 19 (2003) 691.

[23] H.R. Krall, IEEE Trans. Nucl. Sci. NS-14 (1967) 455.

[24] J.D. Lewin, P.F. Smith, Astropart. Phys. 6 (1996) 87.

[25] S. Agostinelli, et al., Nucl. Instrum. Methods A 506 (2003) 250, see also, http://geant4.web.cern.ch/geant4.

[26] R. Bernabei, et al., Phys. Lett. B 389 (1996) 757.